EVOLUTION AND GROWTH OF LARGE SCALE STRUCTURES IN HIGH COMPRESSIBILITY MIXING LAYERS

Tobias Rossmann, M. Godfrey Mungal, and Ronald K. Hanson
Department of Mechanical Engineering, Stanford University
Stanford, California 94305-3032 USA
rossmann@stanford.edu

ABSTRACT

The basic physical mechanisms for shear layer growth have been shown in computations to change at very high compressibilities. A double diaphragm, shock tunnel driven hypersonic mixing layer facility is used to reach compressibility levels not possible in blowdown-type facilities. Mixing layers at M_c = 0.8 and 1.7 are examined in streamwise, plan, and end views using Schlieren and acetone PLIF imaging schemes. Analysis of these images yields normalized shear layer growth rates, concentration information on the fast side of the shear layer, and visualization of the behavior of large scale structures. Normalized growth rate data is reported for M_c = 0.8 – 2.7 as derived from averaged schlieren images.

INTRODUCTION

Interest in producing air-breathing engines for hypersonic flight has stimulated fundamental research efforts into the effect of scalar mixing at high Mach numbers. Although the geometry of new fuel injection strategies are likely to be complex and three-dimensional in nature, studies of simple shear flows are necessary to gain an understanding of the fundamental effect of compressibility on mixing and combustion. This information about compressible turbulence can then be used to improve scramjet combustor designs.

The two-dimensional mixing layer is the most fundamental flowfield in which the effects of compressibility and large-scale structure on turbulent mixing can be probed. Prior investigations have delved into the growth and evolution of large-scale structures (Clemens and Mungal, 1995; Papamoschou and Roshko, 1988), their convection velocity (Fourgette, *et al.*, 1990; Papamoschou and Bunyajitradulya, 1997), and how they interact with the mean velocity field (Urban, *et al.*, 1998). While many of these experimental and computational examinations have led to an increased understanding of mixing at low to moderate compressibility conditions, few experimental works have focused on the higher compressibility regime.

In this study, the organization and character of large-scale structures at two higher compressibility conditions are examined in detail using laser-based diagnostics. As scalar structures have been shown in numerical simulations to become more three-dimensional with increasing compressibility (Day, *et al.*, 1998; Freund, *et al.*, 2000; Sandham and Reynolds, 1991), spatially resolved visualization techniques are necessary to determine the dimensionality and extent of these structures (Seitzman, *et al.*, 1994). Images from line-of-sight integrated techniques can be misleading, either lacking the resolution to capture the structures or masking the large-scale structure with smaller turbulent eddies.

EXPERIMENTAL DETAILS

The shock tunnel driven mixing layer facility (Rossmann, *et al.*, 1999) along with the PLIF and schlieren diagnostics (Rossmann, *et al.*, 2001) used for these measurements have been described in detail previously, and are briefly reviewed here.

Reflected Shock Tunnel

The shock tunnel facility consists of a 2.6m long driver section (18 cm internal diameter) and a 9.1m long driven section (11.4 cm internal diameter). A 10 cm x 5 mm slot is cut into the endwall to form the throat for the various nozzles that are coupled to the shock tube. The tunnel is designed to handle pressures up to 150 atm, which allows for cross flows in the mixing layer facility of up to Mach 6 at test section pressures of at least 0.1 atm.

The mixing layer facility (Figure 1) houses a supersonic nozzle (which draws from the shock tunnel), a splitter plate, a subsonic nozzle, and a low speed manifold used to inject the subsonic portion of the mixing layer. This low-speed portion is provided

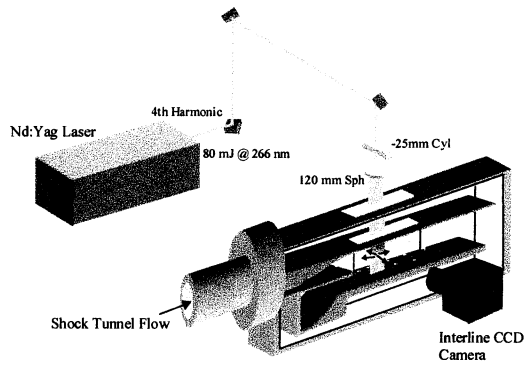

Figure 1 : Shock tunnel schematic showing the optical setup for side view acetone PLIF imaging.

by a small blow down tank, which is activated 200-300 msec before the firing of the shock tube to allow adequate time for the flow to develop. The exit of the mixing facility is joined to a 3 m^3 dump tank, which is used to maintain a constant test section pressure during the test time.

Acetone PLIF System

The frequency quadrupled output of a Nd:YAG laser was used as the excitation source. The laser had a pulse width of 6 nsec and pulse energy at the test section of 16-18 mJ. The beam was formed into a sheet (160 μm x 50 mm) using a cylindrical and spherical lens combination (Figure 1). The sheet was directed into the test section either from above (for side view imaging) or from the side (for plan and end view imaging). Sheet thickness and size did not vary significantly between these orientations

Acetone vapor, seeded to a mole fraction of 23% into the shock tunnel test gas by the use of a pressurized acetone bubbler, was shock heated to 1100 K and 25 atm. At these conditions, the acetone pyrolysis lifetime is approximately 10 msec (Lozano, *et al.*, 1992), while the shock tunnel test time is only 1.5 msec. Thus, only about 14% of the initially seeded acetone is lost to the pyrolysis reactions. However, above 1200K, over 95% of the seeded acetone will decompose. This effectively limits the maximum Mach number that can be used with supersonically seeded acetone PLIF. In order to not lose large amounts of acetone to pyrolysis or condensation in the expanded state, the test section Mach number cannot exceed five.

The resulting fluorescence signal was imaged onto an un-intensified interline CCD camera (1300 x 1030 array with 6.8 μm pixels) equipped with a 50 mm f/1.2 camera lens. The exposure of the CCD array was gated to 2 μsec by using the electronically shuttered first image of the frame transfer mode. Shot-to-shot laser power fluctuations were monitored by a 1 mm photodiode with a phosphor mask.

Data Reduction

The raw fluorescence images were corrected for camera dark background, non-uniform spatial response of the camera/collection optics, and spatial distribution of the laser energy. Instantaneous sheet corrections were performed in the side view images only, as the plan and end views do not possess uniformly seeded regions that span the laser sheet. For those views, 10 frame average sheet correction images were collected by uniformly seeding the entire test section with acetone. The processed images were binned 3x3 to improve signal to noise ratio, leading to a resolution in the side and plan views of approximately 160 x 120 x 120 μm. The peak signal to noise ratio for the side view images is 15 at the lowest convective Mach number conditions. At higher convective Mach numbers, the overall pressure in the test section is decreased along with the peak SNR.

Because the end view images were taken at an angle of 37 degrees to the flow axis, these raw images appear distorted. A transfer function between off-axis and on-axis imaging was experimentally found by imaging a plate with concentric squares at the skewed angle. This function was then used to correct the end view images by stretching the axes to make the images appear rectilinear. The end view resolution is 160 x 300 x 300 μm, and the peak SNR for these images is 10.

RESULTS AND DISCUSSION

Growth Rate

Schlieren imaging results were obtained for a wide range of convective Mach numbers (0.8 – 2.7) using a high framing-rate camera. The resolution of the schlieren image is quite coarse compared to the PLIF technique (0.5 x 0.5 mm); however, for determining the overall growth rate and examining the dynamics of the large-scale structures, this resolution is sufficient. These images are gated to 250 nsec and are spaced 4 μsec apart. Consequently, the motion of the fastest velocity scales is less than one pixel during the imaging time.

The growth rate of the mixing layer was estimated by fitting envelope lines to the visual extent of the shear layer in an eight or sixteen frame average image. Although the procedure is somewhat subjective, repeated measurements using different nozzles and side-two gas composition give low scatter. Growth rate data from M_c = 0.8 to 2.0 were taken using a Mach 3.0 nozzle with nitrogen on the fast side and from M_c = 1.2 – 2.7 using a Mach 5.0 nozzle with argon as the high-speed gas.

Uncertainty in the convective Mach number is minimized by careful measurement of the pressures and Mach numbers in each section of the shock tunnel. Shot variations in the incident Mach number in the shock tunnel can vary the nozzle stagnation pressure by as much as 3% and the stagnation temperature by 2%. However, since the Mach

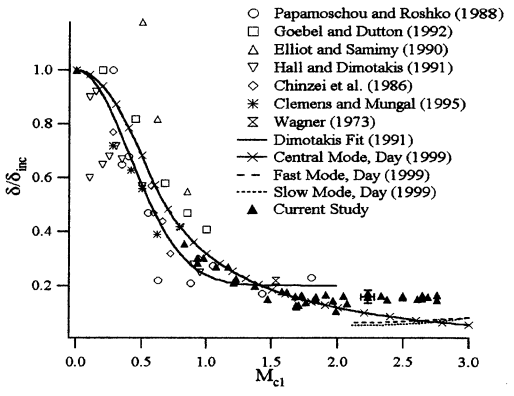

Figure 2 : Experimental and computational normalized growth rate data for compressible mixing layers vs. convective Mach number.

Figure 3 : Instantaneous schlieren image of M_c = 0.8 mixing layer case. Imaged region is 23 x 8 cm. s = 0.23, r = 0.07.

number of each nozzle is precisely calibrated using pitot probe and Mach angle data, the uncertainty of the convective Mach number can be reduced to 1.5% for most cases.

In Figure 2, normalized growth rate data from several investigators are shown plotted versus the convective Mach number. Fairly good collapse has been noted in the M_c = 0 – 1.0 range accessible by those researchers using blow-down wind tunnels. Current experimental data follows closely the central mode growth rate decay of a recent linear stability analysis (Day, *et al.*, 1998). As will be shown clearly in the PLIF images, centralized structures play a diminished role in the entrainment behavior of the mixing layer above M_c = 1.0. However, the growth rate suppression of this central mode appears to be a good description of the overall growth rate trend up to M_c = 2.0.

Above a convective Mach number of 2, the normalized growth rate is nearly constant at a value of δ/δ_{inc} = 0.16. One possible explanation for this behavior is the saturation of the growth rate suppression mechanism at this very high shear rate. Any further increases in convective Mach number could result in physical changes to the mixing layer that do not manifest themselves in the overall layer growth rate, e.g. a shift to purely three-dimensional streamwise large-scale structures. Another possible explanation, which supports current numerical results, is that the central mode structure is transitioning to a three-dimensional co-layer structure as described by Day et. al. (1998). In that physical model, co-layer growth modes, which have reduced shear across the scalar structures and a convective velocity preference for a particular free stream, begin to become a more important entrainment mechanism. The modes have been shown to become active numerically above M_c = 2.0 and dominate the overall layer growth rate above M_c = 3.0. However, it is yet unclear whether these modes can ever exist in a two-dimensional state experimentally (i.e. not oblique) and thus be discerned from purely streamwise structures.

M_c = 0.8

This test condition is generated by creating an 1100 K, 25 atm stagnation region in the shock tunnel with a test time of 1.5 msec. This high enthalpy gas feeds a Mach 3 supersonic nozzle, which expels into

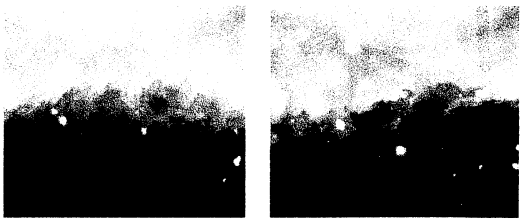

Figure 4 : Instantaneous acetone PLIF side view images of M_c = 0.8 mixing layer case. Imaged region (4.5 x 4 cm) is 18 cm downstream of the splitter tip.

a backpressure of 0.37 atm. The dump tank pressure is held lower than the ideally expanded backpressure to allow for a proper mixing layer to form with no waves launched from the splitter tip. A low-speed flow of helium moving at 90 m/sec mixes with the supersonic, high-speed flow of 20% acetone, 80% air traveling at 1250 m/sec to form a M_c = 0.8 mixing layer.

An instantaneous side view schlieren image of the lowest convective Mach number case looked at in this study is shown in Figure 3. The mixing layer has little discernable large-scale structure evident in this line-of-sight integrated technique. Some darker bands, which are apparent towards the end of the image, suggest some large-scale structure is possibly contained inside the layer and is obscured by the sensitivity of the schlieren technique. However, individual structure is clearly evident in the PLIF views.

PLIF Side View. Shown in Figure 4 is a single-shot set of acetone PLIF images taken at 18 cm downstream of the splitter plate. All the images are from separate firings of the shock tunnel and the flow is from left to right. Some structure is evident within the images, but a mostly jagged interface is seen between the high-speed side and the mixing layer, which is consistent with previous findings. Few regions of pure low-speed fluid near the high-speed interface are found in these images. Thus, the entrainment mechanism of this layer is still predominantly controlled by large roller structures, though they might be more three-dimensional in nature (Clemens and Mungal, 1995).

PLIF Plan View. Imaging in this plane allows for the observation of a dominant disturbance angle of the large-scale structure. In previous, less compressible work, this view demonstrated to researchers the transition to oblique downstream propagation of the rollers at $M_c > 0.6$.

Plan views for the M_c = 0.8 case are shown in Figure 5, 18 cm downstream and at the height of the splitter plate. The flow direction here is still left to right. These images reveal a highly three-dimensional structure when compared to lower compressibility cases. No dominant two-dimensional structures are apparent; however, there is some evidence (particularly in the upper left hand corner image) of small-scale mushroom structures, as in

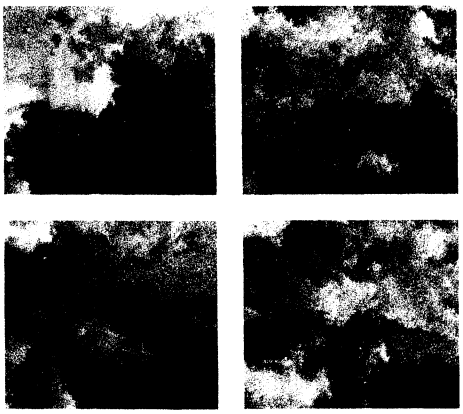

Figure 5 : Instantaneous acetone PLIF plan view images of M_c = 0.8 mixing layer case. Imaged region (4.5 x 4 cm) is 18 cm downstream of the splitter tip, along the mid-plane of the mixing layer.

incompressible mixing layers. In general, these plan view images appear highly three-dimensional and lacking in any spatial regularity or organization.

PLIF End View. Figure 6 shows instantaneous end view PLIF images of the M_c = 0.8 case imaged at the same downstream location (18 cm) as the plan and side views. Due to shot-to-shot variations in the laser intensity profile, these images exhibit some sheet correction noise, which appear as horizontal bands, since they are corrected using an average sheet intensity profile. Also, because of the non-linear stretching of the image due to the angle between the imaging axis and the laser sheet, the right-hand side of the images appears a bit out of focus. Reducing the off-axis imaging angle to the smallest value allowed by the experimental setup minimized this problem.

All of the end views appear to show highly convoluted structures. There are both larger (~δ) and smaller size structures in evidence. As were seen in the plan view, images again feature small mushroom type structures possibly caused by small-scale counter-rotating vortices. These small and large-scale structures also appear to be mixed internally, rather than jets of pure high-speed or low-speed fluid protruding into the free stream, consistent with the observations made in the side view plane.

M_c = 1.7

This test condition is generated using the same

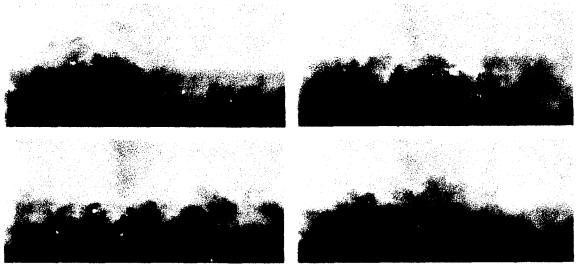

Figure 6 : Instantaneous acetone PLIF end view images of M_c = 0.8 mixing layer case. Imaged region (10 x 4 cm) is 18 cm downstream of the splitter tip.

Figure 7 : Instantaneous schlieren image of M_c = 1.7 mixing layer case. Imaged region is 23 x 8 cm. s = 1.57, r = 0.02.

shock tunnel running conditions as the M_c = 0.8 case. However, in this case, the lower speed flow is air traveling at 30 m/sec at a reduced backpressure of 0.3 atm. One distinct advantage of a shock tunnel facility over a blowdown facility is the ease of changing convective Mach numbers. Since the amount of gas required for side-two injection is quite small, changing the low-speed side gas supply, and thus M_c, is simple and swift.

Figure 7 shows an instantaneous side-view schlieren image of the M_c = 1.7 case, from x = 0 to 23 cm downstream. The mixing layer does not resemble lower compressibility conditions, as there appears to be little large-scale centralized structure. Much of the evident structure is in the form of streamwise tongues of mixed fluid, which protrude into both the high- and low-speed side. These jets also appear to have a preferred orientation that is approximately equal to the Mach wave angle of the convective Mach number. Strong coupling between the radiation field and the scalar structure has been shown previously, both experimentally (Rossmann, *et al.*, 2001) and computationally (Freund, *et al.*, 2000; (Lessen, *et al.*, 1966). Further evidence of the streamwise nature of the structures and their interaction with radiated Mach waves is available in the PLIF views.

PLIF Side View. Figure 8 shows single-shot acetone PLIF images taken at 18 cm downstream of the splitter plate. Immediately apparent in the image, different from the M_c = 0.8 case, are the bright streaks, which emanate from the mixing layer and

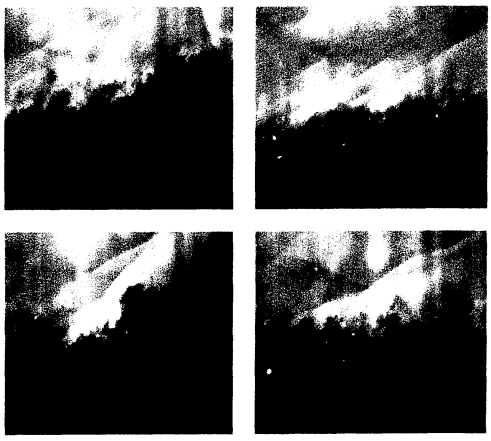

Figure 8 : Instantaneous acetone PLIF side view images of M_c = 1.7 mixing layer case. Imaged region (4.5 x 4 cm) is 18 cm downstream of the splitter tip.

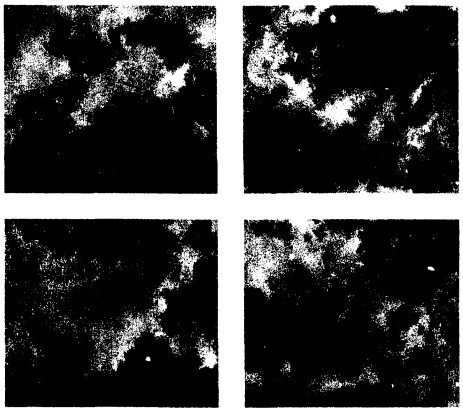

Figure 9 : Instantaneous acetone PLIF plan view images of M_c = 1.7 mixing layer case. Imaged region (4.5 x 4 cm) is 18 cm downstream of the splitter tip along the mid-plane of the mixing layer.

propagate into the free stream. These bright streaks are Mach wave radiation, which originates from the shear layer. They occur because the difference between the convection velocity of the propagating large-scale structures and the velocity of the fast stream is greater than the local freestream speed of sound. Thus, the large structures act locally as bluff bodies in the flow and the entire fast-side interface can be thought of as a "wavy" wall in supersonic flow, radiating Mach waves whose angle is defined by the local velocity difference.

The side views also demonstrate that large amounts of pure low-speed fluid can be found adjacent to the high-speed interface. This type of scalar structure is consistent with three-dimensional streamwise structures, which engulf large amounts of freestream fluid and then transport it to the other side of the mixing layer. However, the true three-dimensionality of these structures is only evident in the other imaging views.

PLIF Plan View. Plan views for the M_c = 1.7 case are shown in Figure 9, 18 cm downstream and at the height of the splitter plate. The images presented here show highly convoluted three-dimensional structure consistent with strong streamwise motions. Structures composed primarily of either high- or low-speed fluid are prevalent, stacking on top of each other; this observation is consistent with numerical simulations at a similar convective Mach number (Freund, *et. al.*, 2000). Little evidence of two-dimensional structure (oblique or spanwise oriented) is present.

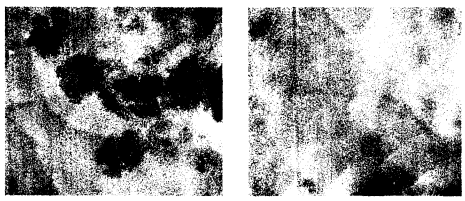

Figure 10 : Instantaneous acetone PLIF plan view images. Left image is taken at z =+ 0.5 cm above the splitter tip, right image at z = +1.0 cm.

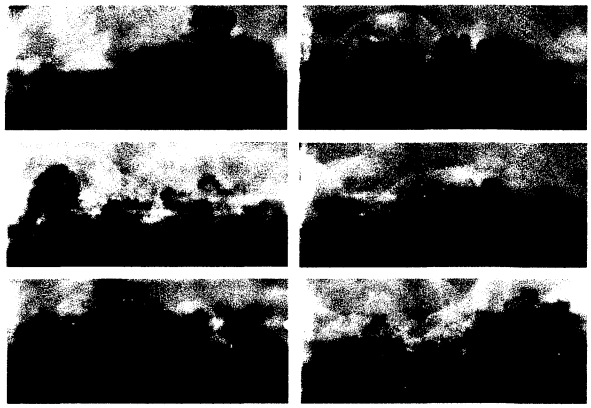

Figure 11 : Instantaneous acetone PLIF end view images of M_c = 1.7 mixing layer case. Imaged region (10 x 4 cm) is 18 cm downstream of the splitter tip.

A more informative impression of the nature of the radiated Mach waves can be obtained from plan view cuts taken above the shear layer centerline. Figure 10 shows instantaneous images taken near the high-speed interface of the shear layer and just above it. The true three-dimensionality of the streamwise structures is unmistakable in the left image where several elongated structures are clear. Also, the structures appear to act as bluff bodies in the flow, with bow shock waves surrounding the large-scale structures. Further into the free stream, above the level of the mixing layer, the complexity of the radiation field is evidenced by many Mach wave structures, which emanate from the mixing layer, reflecting in the test section.

PLIF End View. Figure 11 shows instantaneous end view PLIF images of the Mc = 1.7 case imaged at 18 cm downstream from the splitter tip. The horizontal streaks due to variation in the sheet intensity profile here are more pronounced than the M_c = 0.8 case due to decreased signal to noise ratio.

In this set of images, the streamwise character of the structures is pronounced, and elevated levels of spanwise asymmetry are prevalent. Consistent with the other imaging planes, three-dimensional scalar structures consisting of mostly low-speed side fluid are seen reaching into the fast-side freestream. Similar bluff body shock wave behavior is also evident, especially in the images on the right hand side.

M_c = 2.7

This test condition is generated by creating a 2700 K, 31 atm stagnation region in the shock tunnel with a test time of 1.7 msec. This high enthalpy gas feeds a M = 5 supersonic nozzle which expels gas into a backpressure of 0.09 atm. The dump tank pressure is again held lower than the ideally expanded backpressure to minimize waves launched from the splitter tip. A low-speed flow of carbon dioxide moving at 75 m/sec mixes with the supersonic, high-speed flow of argon traveling at 1600 m/sec to form a M_c = 2.7 shear layer.

Figure 12 : Instantaneous schlieren image of M_c = 2.7 mixing layer case. Imaged region is 23 x 8 cm. s = 0.96, r = 0.05.

Figure 12 shows an instantaneous side-view schlieren image of the M_c = 2.7 case, from x = 0 to 23 cm downstream. The shear layer appears to have little strong streamwise structures in evidence. This image resembles the low convective Mach number case, with only minor three-dimensional structure apparent. However, only spatially resolved techniques can be used to draw conclusions about the scalar structure of the mixing layer, since schlieren images can often be misleading, especially in highly three-dimensional flow fields. There is also strong Mach wave radiation in this flow field as in the M_c = 1.7 condition, though it is not shown in these schlieren images. Further study using PLIF imaging of nitric oxide is needed to examine the dynamics of the large-scale structures at this very high convective Mach number condition.

CONCLUSIONS

Mixing layers at convective Mach numbers of 0.8 and 1.7 were imaged in three different views using acetone PLIF. Normalized growth rates for compressible shear layers are reported for M_c = 0.8 to 2.7. These growth rates support the trend suggested by earlier numerical work.

In the lower compressibility case, M_c = 0.8, studied here, the high-speed side interface is jagged and convoluted with small mushroom-shaped jets protruding into the shear layer. These jets are mostly mixed and have some three-dimensional character to them, as shown in multiple views.

For the higher compressibility case, M_c = 1.7, thin streamwise vortical structures dominate the flow topology and couple strongly to the Mach wave radiation field. These structures appear to be relatively unmixed, revealing that the streamwise vortices likely engulf fluid from one freestream and transport it rapidly through the layer.

At the highest compressibility case, M_c = 2.7, little streamwise structure is evident in the schlieren images, but ongoing PLIF studies of this conditions will elicit information on the character of the structures at this convective Mach number.

References

Clemens, N. T. and Mungal, M. G., 1995, "Large-scale Structure and Entrainment in the Supersonic Mixing Layer," *J. Fluid Mech.*, Vol. 284, pp. 171-216.

Day, M. J., Reynolds, W. C. and Mansour, N. N., 1998, "The Structure of the Compressible Reacting Mixing Layer: Insights from Linear Stability Analysis," *Phys. Fluids*, Vol. 10, No. 4, pp. 993-1007.

Fourgette, D. C., Dibble, R. W. and Mungal, M. G., 1990, "Time Evolution of the Shear Layer of a Supersonic Axisymmetric Jet at Matched Conditions," *AIAA Journal*, Vol. 10, pp. 157-166.

Freund, J. B., Moin, P. and Lele, S. K., 2000, "Compressibility Effects in a Turbulent Annular Mixing Layer: Part 1. Turbulence and Growth Rate," *J. Fluid Mech.*, Vol. 421, pp. 229-267.

Lessen, M., Fox, J. and Zien, H., 1966, "Stability of the Laminar Mixing of Two Parallel Streams with Respect to Supersonic Disturbances," *J. Fluid Mech.*, Vol. 25, pp. 737-749.

Lozano, A., Yip, B. and Hanson, R. K., 1992, "Acetone: A Tracer for Concentration Measurements in Gaseous Flows by Planar Laser-induced Fluorescence," *Exp. Fluids*, Vol. 13, pp. 369-376.

Papamoschou, D. and Bunyajitradulya, A., 1997, "Evolution of Large Eddies in Compressible Shear Layers," *Phys. Fluids*, Vol. 9, No. 3, pp. 756-765.

Papamoschou, D. and Roshko, A., 1988, "The Compressible Turbulent Shear Layer: An Experimental Study," *J. Fluid Mech.*, Vol. 197, pp. 453-477.

Rossmann, T., Mungal, M. G. and Hanson, R. K., 1999, "A New Shock Tunnel Driven Facility for High Compressibility Mixing Layer Studies," presented at the *37th Aerospace Sciences Meeting*, Reno, NV, AIAA 99-0415.

Rossmann, T., Mungal, M. G. and Hanson, R. K., 2001, "Acetone PLIF and Schlieren Imaging of High Compressibility Mixing Layers," presented at the *39th Aerospace Sciences Meeting*, Reno, NV, AIAA 2001-0290.

Sandham, N. D. and Reynolds, W. C., 1991, "Three-Dimensional Simulations of Large Eddies in the Compressible Mixing Layer," *J. Fluid Mech.*, Vol. 224, pp. 133-158.

Seitzman, J. M., Miller, M. F., Island, T. C. and Hanson, R. K., 1994, "Double-pulse Imaging Using Simultaneous OH/acetone PLIF for Studying the Evolution of High Speed, Reacting Mixing Layers," presented at the *25th International Symposium on Combustion.*

Urban, W. D., Watanabe, S. and Mungal, M. G., 1998, "Velocity Field of the Planar Shear Layer: Compressibility Effects," presented at the *36th Aerospace Sciences Meeting*, Reno, NV, AIAA 98-0697.